Acta Geotechnica (2021) 16:1247–1263
https://doi.org/10.1007/s11440-020-01083-8

RESEARCH PAPER

The 2015 Shenzhen catastrophic landslide in a construction waste dump: analyses of undrained strength and slope stability

Liang-tong Zhan[1] · Xiao-gang Guo[1] · Qian-qian Sun[1] · Yun-min Chen[1] · Zu-yu Chen[2]

Received: 8 March 2020 / Accepted: 12 September 2020 / Published online: 29 September 2020

Abstract
The 2015 catastrophic landslide in a 110-m-high waste dump in Shenzhen is recognized as one of the largest landfill failure worldwide. An earlier comprehensive field investigation revealed that the dominant component of the fill was completely decomposed granite (CDG), and the dumping operation was accompanied by a rise of the groundwater level. In this paper, the complex stress paths for the initially unsaturated fill materials being subjected to both rapid filling and wetting were investigated. A simplified method was proposed for estimating the gain of undrained shear strength under the complex stress paths. Soil samples were taken from the site to a laboratory to measure the undrained shear strength and validate the estimation method. Total stress-based stability analyses were carried out to calculate the factor of safety of the dump at failure. The triggering mechanism of the landslide is clarified as follows: The gain of shear strength with the surcharge loading for the wet layer in the lower part of the waste dump was limited by a build-up of excess pore-water pressure. The gain of shear strength for the relatively dry fill material was attenuated with the rise of groundwater level. When the shear strength was not enough to resist the increasing slip force with the surcharge loading, a deep-seated translational failure took place in the lower wet layer of the waste dump. The proposed method for analyses of undrained strength and slope stability are proven to be applicable to the waste-dumping operation with rapid filling and rising groundwater level.

Keywords Construction waste dump · Completely decomposed granite · Slope stability · Total stress based analysis · Undrained shear strength · Wetting

1 Introduction

Accompanying the rapid urbanization in China in recent years, construction waste (CW) has dramatically increased in many cities. Taking Shenzhen, one of the largest cities in China, as an example, the volume of CW yielded per year was approximately 3.6×10^7 m^3 from 2013 to 2015 [7]. Approximately 61% of the CW was transported to waste dumps for landfilling. More than 40 waste dump sites have been constructed or are planned to be constructed in Shenzhen. As the most common way to dispose of CW, landfilling is often accompanied by the risk of landslides.

✉ Xiao-gang Guo
xiaogang_guo@zju.edu.cn

[1] MOE Key Laboratory of Soft Soils and Geoenvironmental Engineering, Zhejiang University, Hangzhou 310058, China

[2] China Institute of Water Resources and Hydropower Research, Beijing 100044, China

On 20 December 2015, a catastrophic landslide occurred in a 110-m-high waste dump located in Guangming New District, Shenzhen, China. This landslide destroyed 33 buildings and killed 77 people. The characteristics of the landslide were captured by field investigation, unmanned aerial vehicle (UAV) surveys, multistage remote-sensing images and so on [23, 29, 30]. The volume of the sliding mass is approximately 2.51×10^6 m^3. Thus, it is recognized as one of the largest landslides that occurred in a landfill worldwide. The impacted area is 0.38 km^2, with a maximum length of 1100 m and a width ranging from 150 to 630 m. The maximum speed of sliding was estimated to be 50 km/h, and the run-out distance was measured to be approximately 450 m [30].

The post-failure characteristics of this landslide with a high sliding speed and a long run-out distance have motivated the study of the dynamic behaviour using various numerical methods [3, 5, 8, 13, 16, 31]. However, few quantitative analyses were performed to clarify the failure

triggering mechanism of this landslide. This lack of analysis is due to the complexity and uncertainty in the waste dump. The complexity and uncertainty result from the variability in the hydrogeological conditions, and the time-dependent state of the fill materials [30].

Based on a comprehensive field investigation, Zhan et al. [30] reconstituted the geotechnical and hydrogeological conditions of the Guangming waste dump prior to the landslide. The dumping operation was characterized by rapid filling at a rate of 5–7 m/month, inadequate compaction and poor water drainage. The dominant component of the dumped materials was identified to be completely decomposed granite (CDG). The CDG samples taken from the Guangming dump site presented broad grain sizes with the contents of fine-particle (grain size $\leq$ 0.075 mm) greater than 30% [30]. The fill materials with broad grain sizes are probable to have internal erosion and then trigger the instability of slope [24–28]. Actually, fine-grained soil was observed in some sampling boreholes in the middle part of the source area in the field investigation. However, the fine-grained soil samples accounted for less than 3% of the 102 samples and might not form a continuous soil layer [30]. The internal erosion is considered unlikely to be the direct cause of the landslide. The CDG with different initial water contents was dumped in different zones to form a two-zone structure, with high-water-content fill dumped in the lower and rear areas. Inadequate compaction of the fill materials resulted in a low compactness with a relative density (D_r) that ranged from 4 to 67%. No effective drainage facilities resulted in a large quantity of water accumulating in the dump and seeping into the dump, leading to a significant rise in the groundwater level. According to a water balance analysis [30], nearly 70% of the fill was likely to be saturated with the rising of the groundwater level. The rapid landfilling of wet and loose soils very likely caused a build-up of excess pore-water pressure in the poorly drained fill. The existence of excess pore-water pressure in the lower layer of the waste dump was confirmed by a borehole investigation as well as the evaluation of the consolidation degree of the borehole samples [30]. When the dump reached a fill height of 100 m, a deep-seated translational failure occurred in the lower poorly consolidated fill layer.

The above review indicates that the fill materials in the waste dump were initially in an unsaturated state and then experienced a complex stress path involving surcharge loading and wetting prior to the final shearing failure. The surcharge loading caused compression of the pore air and led to partial consolidation of the unsaturated fill, which was poorly drained. The compression and the subsequent wetting resulted in an increase in the saturation degree of unsaturated fill. The change in saturation degree will inevitably alter the shearing behaviour prior to a final failure. In addition, the stress path is believed to be different for the fill materials located in different zones with different initial values of water content. The complex stress path caused a difficulty in the determination of shear strength and the quantitative analysis of slope stability. As noted by Yin et al. [29], conventional methods of stability analysis for natural landslides are difficult to apply to waste dumps because the topography and hydrological conditions were changing during the filling process. The total stress-based method used for the stability analysis of embankments [9] or earth dams [2] under construction cannot be easily implemented for the stability analysis of the waste dump. This is because the determination of undrained shear strength involves the complex stress path of surcharge loading and wetting. Ladd [6] introduced an approach, termed undrained strength analysis (USA), to calculate the gain of shear strength for a saturated cohesive soil ground being subjected to a staged surcharge loading. It was believed that consolidated-undrained shear test (CU) was rational to simulate the staged surcharge loading and failure processes. In the consolidation stage, the K_0 stress condition considering anisotropy was believed to be more rational than the isotropic consolidation. With an interpretation of the CU test results, the relationship between undrained shear strength c_u and vertical consolidation stress σ'_{vc} could be obtained for a stability analysis of the soil ground. To implement the stability analysis, it was required to evaluate the change in vertical effective stress σ'_{vc} in the soil profile during the staged construction. The USA methodology shines a light on the determination of shear strength for the fill materials in this paper, which was subjected to rapid filling under a poorly drained condition.

In this study, the stress paths of the fill materials in the waste dump were identified first by studying the rapid filling process and the rise of the groundwater level. On the basis of the identified stress paths and the methodology of undrained strength analysis, a simplified method was proposed for estimating the undrained shear strength of the fill materials. Then, laboratory tests on the CDG samples taken from the dumpsite were carried out to measure the undrained shear strength. A comparison between the measured and estimated shear strengths was conducted to validate the estimation method. Considering the estimated undrained shear strength, total stress-based stability analyses were carried out to calculate the factor of safety just before sliding. Finally, the influence of the initial saturation degree of the fill materials on the landfill height and capacity was investigated.

2 Stress paths of fill materials in rapid landfilling

As stated above, in this study, the determination of the undrained shear strength involves a complex stress path that reflects surcharge loading and wetting. Therefore, to determine the shear strength, the filling process and the evolution of the groundwater level in the waste dump are clarified as follows.

2.1 Filling process of the waste dump

The geotechnical and hydrogeological conditions of the waste dump reconstructed by Zhan et al. [30] are shown in Fig. 1. The dumpsite was originally an abandoned quarry surrounded by mountains with a narrow opening on the north side. The bedrock was granite and was covered by a layer of spoil waste. The dumping operation began in February 2014. The fill, which mainly consisted of CDG, was stacked first in the front area of the dumpsite. The initial dry density of the fill was assumed to be equal to that of the shallow fill on the front slope, which was not subjected to compaction. The initial dry density was determined to be 1.3 g/cm^3 during the field investigation [30]. The initial water content of the fill in the front area was 19% on average and corresponded to a saturation degree of 48%, as indicated in Fig. 1. Fill with the same composition but a much higher water content was then dumped in the pit surrounded by the front fill and the mountains. The initial water content and the saturation degree of the fill in the pit were determined to be 26% and 66%, respectively, by laboratory tests [30]. As the dumping operation continued, the top of the waste dump reached an elevation of 115 m in November 2014, with an average filling rate of 7 m/month. As shown in Fig. 1, two zones with different initial saturation degrees were formed in the waste dump. It is supposed that a transition zone formed between these zones due to seepage during landfilling. The average values of water content and saturation degree for the transition zone were estimated to be 23% and 58%, respectively. The dumping operation was then suspended by the local government for five months. Operation resumed in April 2015 and continued until the landslide occurred in December 2015. Low-water-content fill was dumped on the upper surface of all three zones in this stage, with a filling rate of 5 m/month. The maximum elevation of the waste dump before the landslide was 160 m. From February 2014 to December 2015, 5.83×10^6 m^3 of fill material was dumped in the quarry site, forming a slope with an overall gradient of 4H/1 V (14°).

2.2 Evolution of groundwater level in the waste dump

Due to the large catchment area and poor drainage, water that accumulated in the waste dump caused the groundwater level to rise during landfilling. The rise of the groundwater level changed the saturation degree of the fill and further altered the stress path and the shear strength. Groundwater level monitoring was absent during the landfilling. The evolution of the groundwater level was computed by conducting water balance analysis and seepage analysis [30]. The water balance analysis was conducted by referring the values of runoff coefficient determined in an imitate rain test [19] and the percentage of infiltration with the effect of topography considered [15, 22].

In accordance with the filling process stated above, the seepage analyses were divided into two stages. The first stage was from February 2014 to March 2015. The maximum elevation of the waste dump reached 115 m in this stage, and then, the dumping operation was suspended for five months. The second stage was from March to December of 2015. The dumping operation was resumed, and the maximum elevation rose to 160 m. Figure 2a indicates the profile of the waste dump for the seepage analysis of the first stage. The bottom *ABCD* is assumed to be an undrained boundary. Water enters the waste dump

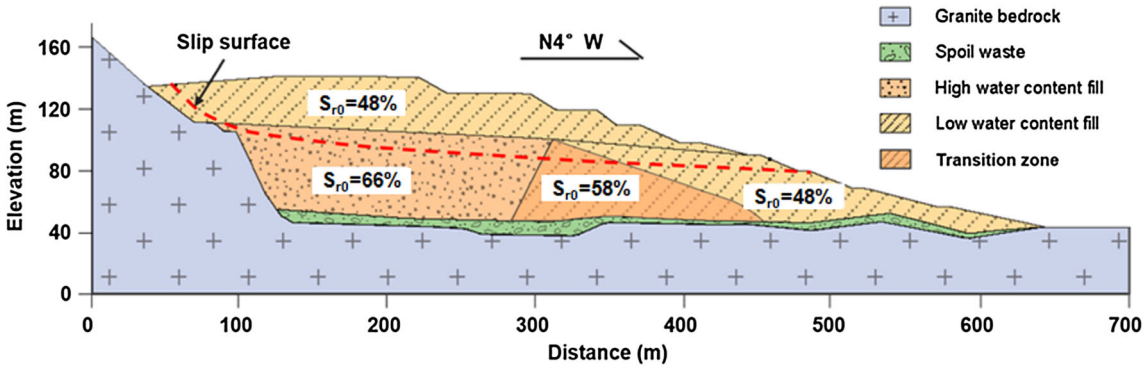

Fig. 1 Representative profile with three zones with different initial saturation degrees

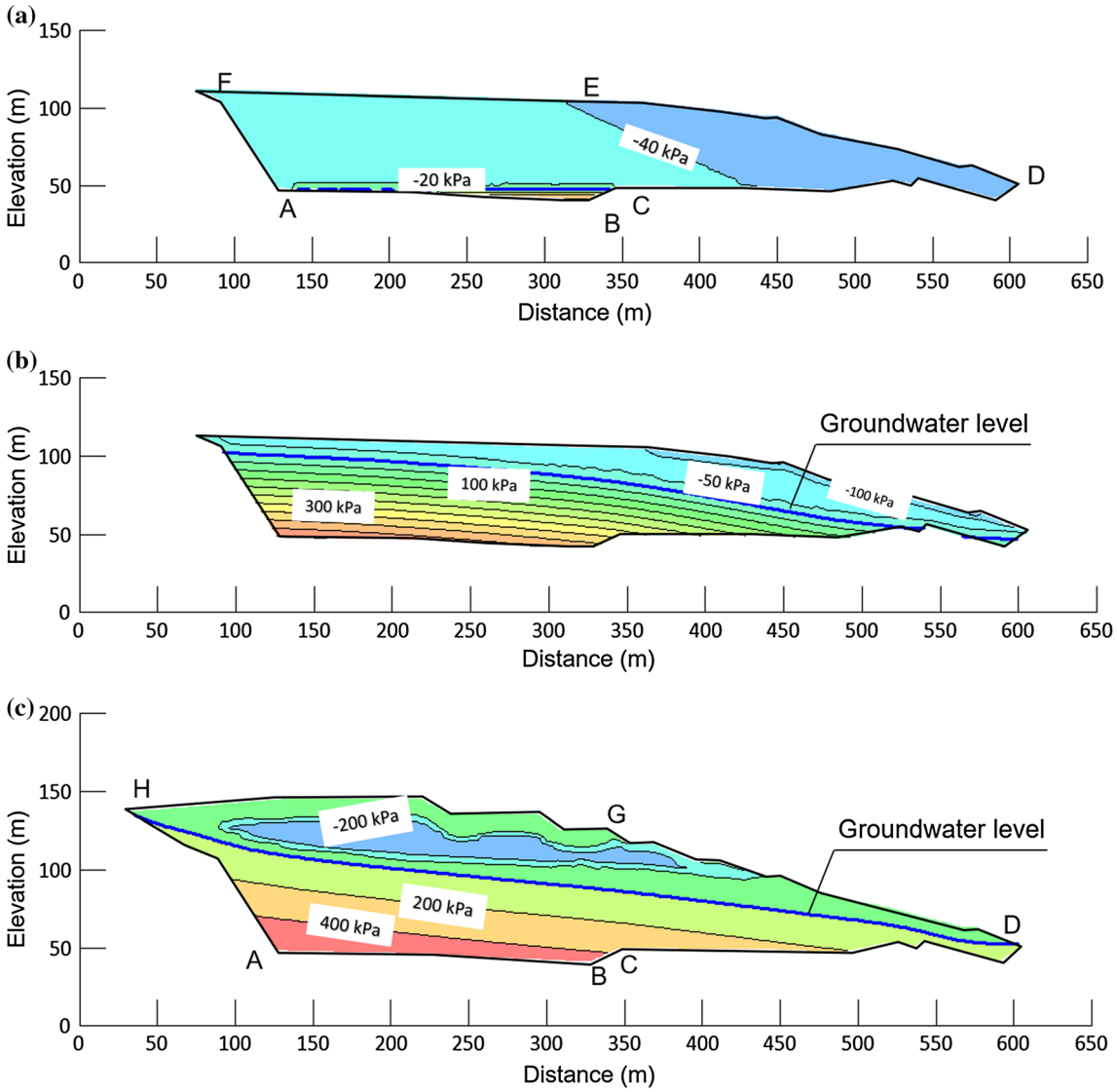

Fig. 2 Groundwater level and pore pressure in the waste dump in (**a**) the initial state, (**b**) the first stage and (**c**) the second stage

along the boundaries *AF* and *DEF*. Before the dumping operation, there was a pond with approximately $9 \times 10^4 m^3$ of water in the quarry site [30]. As the water in the pond was not drained, the initial groundwater level is assumed to be *AC*. The water that accumulated in the waste dump during landfilling consisted of rainfall infiltration in the dumping area and surface and subsurface runoff from the catchment area [30]. It was assumed that 20% [15] of the precipitation in the catchment area became surface runoff and 60% [19] of the surface runoff seeped into the waste dump along the boundary *DEF*, while 7% [22] of the precipitation formed subsurface runoff and infiltrated into the dump along *AF*. In the dumping area, the precipitation on the gentle surface *EF* was believed to infiltrate into the dump totally, while only 20% of the precipitation on the inclined surface *DE* infiltrated into the dump [19]. The evaporation in the dumping area was assumed to be one-third of the evaporation potential from the free water surface (1107 mm/y) [30]. The precipitation and evaporation data during the 22 months before the landslide were collected from the adjacent weather station [29]. In the seepage analysis by the Seep/W module of the software GEO-SLOPE, the infiltration rate was calculated based on the percentages stated above and converted to the unit flux boundary functions for *AF* and *DEF*. The relationship between the permeability coefficient and suction was predicted from the measured soil water characteristic curve (SWCC), and van Genuchten's model was used for the prediction [4]. The relationship of volumetric water content and permeability coefficient to suction for the CDG with a dry density of 1.3 g/cm^3 is listed in Table 1.

Table 1 Relationships of volumetric water content and permeability coefficient to suction for the CDG

Volumetric water content	0.515	0.498	0.413	0.360	0.313	0.293	0.272	0.250
Suction (kPa)	0.1	10	50	100	209	305	500	1000
Permeability coefficient (m/s)	1.67E−06	3.72E−07	2.19E−08	3.18E−09	3.21E−10	9.48E−11	1.88E−11	1.91E−12

The computed groundwater level from the first stage of seepage analysis is shown in Fig. 2b. A significant rise of the groundwater level was caused by the residual water ponding in the quarry and the subsequent water accumulation in between February 2014 and March 2015. It can be seen that the rise of groundwater level makes the fill materials in the rear part saturated. Figure 2c shows the profile of the waste dump for the second stage of seepage analysis. The updated boundaries *AH*, *DG* and *GH* have the same percentages of infiltration as those of *AF*, *DE* and *EF*, respectively. The computed groundwater level from the second stage of seepage analysis is shown in Fig. 2c. Further rise of groundwater level was observed during the second stage of filling. The groundwater level at the front was close to the slope surface, which was consistent with the field observation by the staff at the site.

2.3 Stress paths for different zones of the waste dump

The stress paths of the fill during the landfilling were identified based on the filling process and the groundwater level evolution. According to the initial values of saturation degree and the change in groundwater level for the two stages, the cross section of the waste dump before failure is roughly divided into 14 zones, which are shown in different colours in Fig. 3. Different zones have different stress paths.

Two stress state variables for unsaturated soil mechanics, i.e., net normal stress $(p - u_a)$ and matrix suction $s = u_a - u_w$, are used to interpret the stress path involving surcharge loading and wetting (see Fig. 4). Taking Zone 2 and Zone 12 in the waste dump as examples, the stress paths are shown in Fig. 4a and b. For the unsaturated fill dumped in Zone 2, as indicated by point A in Fig. 4a, the net normal stress $(p - u_a)$ and shear stress q were zero

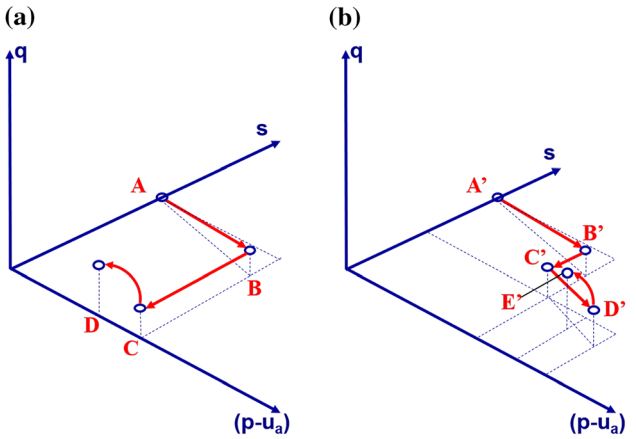

Fig. 4 Schematic diagram of the stress paths for (**a**) Zone 2 and (**b**) Zone 12

initially, while the matrix suction s had a specific value. The dumping operation imposed surcharge loading on the fill and led to increases of $(p - u_a)$ and q, as indicated by path AB. The matrix suction decreased slightly as the saturation degree increased with a soil compression. A subsequent wetting with the rise of the groundwater level made the fill in Zone 2 saturated. The matrix suction decreased to zero, as indicated by the path BC. It was supposed that the wetting due to a rise of the groundwater level did not lead to a collapse in the fill. This process did not include compression, so $(p - u_a)$ and q remained constant. In the case of poor drainage, the subsequent surcharge loading resulted in a built-up of excess pore-water pressure in the saturated fill. The fill was subjected to rapid shearing during the landslide. The shear stress increased dramatically to point D, which was on the failure envelope. For the fill in Zone 12, during the filling process, the groundwater level approached this zone gradually. The upward movement of water due to capillary rise reduced the matrix suction, as indicated by B'C' in Fig. 4b. The

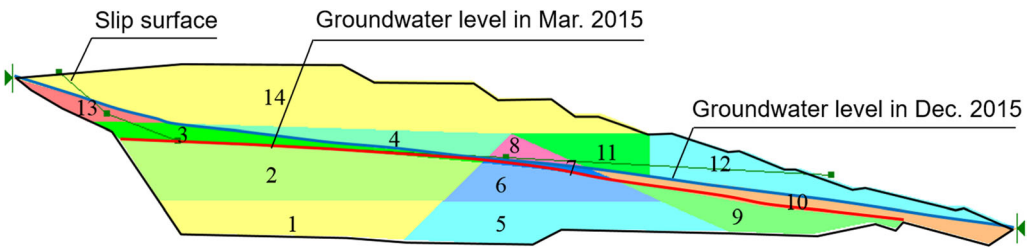

Fig. 3 Discretization of the cross section of the waste dump prior to sliding

succeeding dumping operation further compressed the fill, as indicated by C'D'. The unsaturated fill in Zone 12 was finally subjected to rapid shearing. The stress state changed to point E' on the failure envelope. The final stress states for the fill in Zones 2 and 12, i.e., points D and E', indicate different shear strengths. It is anticipated that the fill with a lower initial saturation degree is more compressible under undrained conditions and thus has higher shear strength. The stress paths for the other 12 zones are interpreted in a similar way. This stress path interpretation provides insight into the estimation of undrained shear strength for fill materials.

3 Estimation of undrained shear strength

Figure 5 shows the evolution of total stress state and hydraulic state for the soil element being subjected to the rapid filling under a poorly drained condition. The evolution basically involved three kinds of loading process, i.e., surcharge loading due to dumping operation, wetting due to groundwater rise and shearing at failure. The surcharge loading caused an increase in vertical total stress and saturation degree S_r. The rapid loading process can be assumed to be an undrained compression. The wetting led to an increase in saturation degree S_r and a decrease in matrix suction s. It was assumed that no volume change occurred in the wetting process. The final dumping operation caused a shearing failure of the soil element. It is assumed to be an undrained shearing without volume change because the saturation degree in the soil element reached a high value and the failure was rapid. It should be noted that the surcharge loading and wetting might occur multiple times during the landfilling. Thus, the stress path for the soil element can be simplified to be an undrained compression, a wetting and a final undrained shearing. The in situ stresses at the compression stage were believed more close to K_0 condition. The K_0 consolidation could be approximately equivalent to an isotropic consolidation with a confining pressure $\sigma_3 = \sigma_{vc}(1 + 2K_0)/3$. σ_{vc} is the vertical total stress, and K_0 is the coefficient of earth pressure at rest. The effective consolidation stress at the compression stage could be determined by an estimation of pore pressure by assuming an undrained isotropic compression. During the wetting stage, the decrease in suction can be estimated from SWCC, and the contribution of residual suction to shear strength can be evaluated by the suction-induced stress [10]. Based on these simplifications, the gain of undrained shear strength for the soil element during the landfilling can be estimated in accordance with the USA methodology. The estimation procedure of undrained shear strength includes the following three steps.

a. Step 1: estimation of pore pressure generated during undrained isotropic compression.

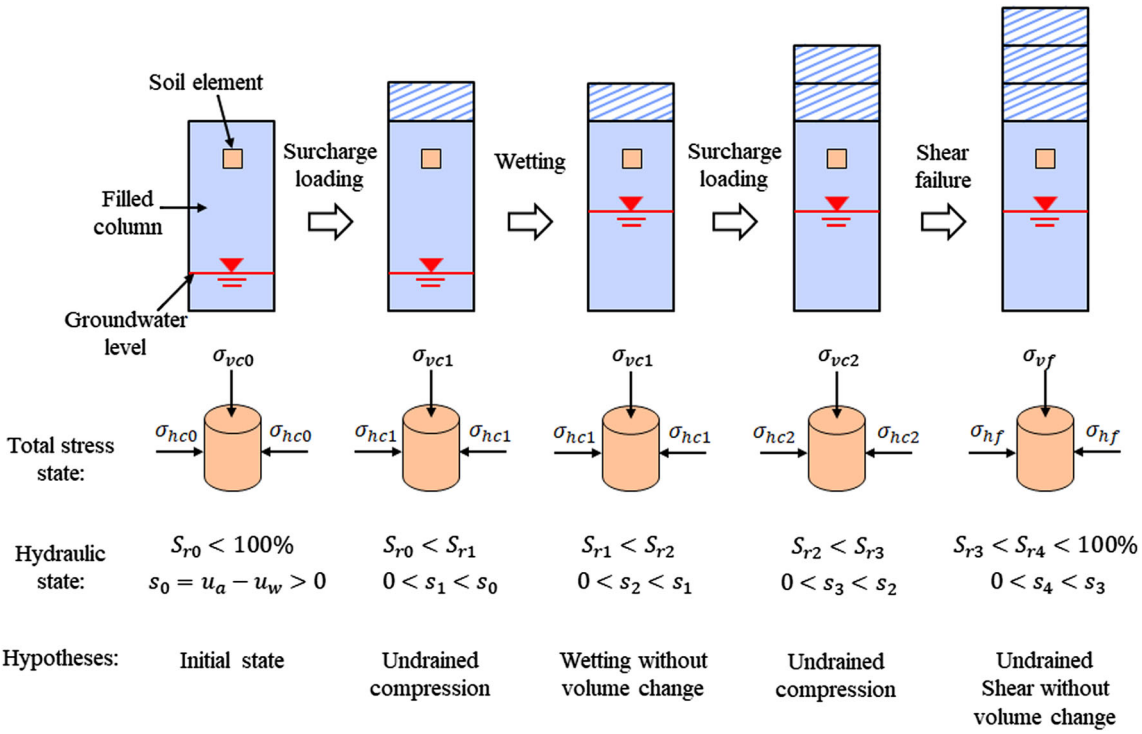

Fig. 5 Total stress state and hydraulic state of soil element during rapid landfilling

For isotropic compression, Skempton [17] gave an expression of the pore pressure coefficient B as

$$B = \frac{\Delta u_{aw}}{\Delta \sigma_3} = \left(1 + n_0 \frac{C_{aw}}{C_s}\right)^{-1} \tag{1}$$

in which Δn is the change in porosity. In the definition of C_{aw} given by Skempton and Bishop [18], the pore air and pore water were treated as a fluid mixture. In other words, the pore-air pressure was assumed to be equal to the pore-water pressure. The influence of the surface tension was disregarded. By taking Boyle's and Henry's laws into account, Schuurman [14] derived an expression of the compressibility of the water/air mixture as

$$C_{aw} = (1 - S_{r0} + h \cdot S_{r0})\left(u_{a0}/u_a^2\right) \tag{3}$$

where u_{a0} is the initial pore-air pressure; u_a is the pore-air pressure after loading and equals $(u_{a0} + \Delta u_a)$; S_{r0} denotes the initial saturation degree; and h is the solubility of air in water and equals 0.02 at 20 °C. Considering Eq. (1), the change in pore pressure is expressed as

$$\begin{aligned} \Delta u_{aw} &= \Delta u_a \\ &= \left[1 + n_0 \frac{(1 - S_{r0} + h \cdot S_{r0})\left(u_{a0}/u_a^2\right)}{C_s}\right]^{-1} \Delta \sigma_3. \end{aligned} \tag{4}$$

In undrained isotropic compression, the water content remains constant. The saturation degree after loading is determined by

$$S_{ri} = \frac{S_{r0} e_0}{e_i} \tag{5}$$

in which e_0 is the initial void ratio and e_i is the void ratio after the i-th loading and expressed as

$$e_i = e_0 - (1 + e_0)(1 - B)\Delta \sigma_3 \cdot C_s. \tag{6}$$

The pore pressure is determined by iterative calculation of Eq. (4). The initial saturation degree and pore pressure are updated via Eqs. (5) and (6) in each iteration step. Notably, neglecting surface tension is more acceptable in the case with a high saturation degree, in which pore air is assumed to exist in pore water in the form of bubbles.

b. Step 2: estimation of effective consolidation stress $\sigma_3^{'}$ by taking the contribution of suction into account.

Although the effect of surface tension (or matrix suction) was ignored in the calculation of pore pressure, the contribution of suction to the shear strength should be taken into account for an unsaturated fill. To determine the shear strength, the effective consolidation stress prior to shearing should first be identified. In the equation of shear strength proposed by Vanapalli et al. [20], the effective consolidation stress with a contribution of suction was expressed as

$$\sigma_3^{'} = (\sigma_3 - u_a) + S_e(u_a - u_w) \tag{7}$$

where S_e is the effective saturation and u_w is the pore-water pressure. Lu et al. [11] determined the effective saturation by employing van Genuchten's model for the SWCC, i.e.,

$$S_e = \frac{S_r - S_{\text{res}}}{1 - S_{\text{res}}} = \left[\frac{1}{1 + (\alpha \cdot s)^{\beta}}\right]^{\frac{\beta - 1}{\beta}} \tag{8}$$

where S_{res} is the residual saturation, α and β are the fitting parameters determined by SWCC [18], and s is the matrix suction. $S_e(u_a - u_w)$ is an approximation for the contribution of suction to effective stress [10].

Once the saturation degree is determined, the effective consolidation stress can be determined by Eq. (7).

c. Step 3: estimation of undrained shear strength via the modified Cam-Clay model.

After undrained isotropic compression and wetting, the fill was assumed to be saturated or nearly saturated. From the modified Cam-Clay model, the volume change in the saturated soil in the undrained shear is

$$\begin{aligned} d\varepsilon_v = &\frac{1}{(1 + e_0)p'}\left\{\left[\kappa + (\lambda - \kappa)\frac{M^2 - \eta^2}{M^2 + \eta^2}\right]dp' \right. \\ &\left. + (\lambda - \kappa)\frac{2\eta}{M^2 + \eta^2} dq\right\} \\ &= 0 \end{aligned} \tag{9}$$

in which p' is the mean effective normal stress; λ and κ are the slopes of the normal consolidation line and unloading/reloading line in the coordinate of e versus lnp', respectively; M is the slope of the critical state line in the coordinate of q versus p'; η is the stress ratio determined by $\eta = q/\left(p' + p_r'\right)$ and equal to M at failure; p_r' denotes the equivalent normal stress of cohesion and equals $c'/\tan\varphi'$ [1]; and q is the deviatoric stress. Equation (9) leads to

$$\frac{dq}{dp'} = K\frac{\left(p' + p_r'\right)}{q} + H\frac{q}{\left(p' + p_r'\right)} \tag{10}$$

where

$$K = \frac{\lambda M^2}{2(\kappa - \lambda)}$$

and

$$H = \frac{(2\kappa - \lambda)}{2(\kappa - \lambda)}.$$

As the stress state prior to the undrained shear is ($\sigma_3^{'}$, 0), the differential Eq. (10) is solved to obtain

$$\frac{1}{2(H-1)}\ln\left|(H-1)\left(\frac{q}{p'+p_r'}\right)^2 + K\right| = \ln\left(p'+p_r'\right) + \frac{1}{2(H-1)}\ln|K| - \ln\left(\sigma_3^{'}+p_r'\right). \tag{11}$$

At the critical state, the stress ratio is

$$\frac{q}{\left(p'+p_r'\right)} = M. \tag{12}$$

Substituting Eq. (12) into Eq. (11), the shear stress at failure is expressed as

$$q_f = (\sigma_1 - \sigma_3)_f = M \cdot \exp\left[\frac{1}{2(H-1)}\ln\left|(H-1)M^2 + K\right| - \frac{1}{2(H-1)}\ln|K| + \ln\left(\sigma_3^{'}+p_r'\right)\right] \tag{13}$$

or

$$q_f = 2^{\frac{\kappa-\lambda}{\lambda}} \cdot \frac{6\sin\varphi'}{3-\sin\varphi'}\left(\sigma_3^{'} + \frac{c'}{\tan\varphi'}\right). \tag{14}$$

As pointed out by Ladd [6], the USA should attempt to predict the available undrained shear strength on the most realistic potential failure surface, i.e. the surface inclined at $\theta = 45^{\circ} + \varphi'/2$. Therefore, the undrained shear strength was defined as $c_u = q_f \cos\varphi'/2$. Based on this definition, the undrained shear strength is expressed as

$$c_u = 2^{\frac{\kappa-\lambda}{\lambda}} \cdot \frac{3\sin\varphi'\cos\varphi'}{3-\sin\varphi'}\left(\sigma_3^{'} + \frac{c'}{\tan\varphi'}\right). \tag{15}$$

The corresponding normal stress on the most realistic potential failure surface is determined as

$$\sigma_n = \frac{(\sigma_1+\sigma_3)_f}{2} - \frac{(\sigma_1-\sigma_3)_f}{2}\cos\varphi'. \tag{16}$$

The obtained relationship between c_u and σ_n is therefore used in the stability analysis of the waste dump during rapid landfilling. It should be noted that the fill materials with a low initial saturation normally keep unsaturated after undrained compression, and a volume contraction will occur in the undrained shear stage. Thus, the shear strength calculated by Eq. (15) is believed to be underestimated for fill materials with low initial saturation degree. Stability analysis using the underestimated shear strength will yield conservative results.

4 Laboratory measurement of undrained shear strength for the unsaturated fill

The shear strength for the fill material taken from the site of the landslide was measured in the laboratory. The proposed estimation method of undrained shear strength was validated by comparing the estimated strengths with the experimental results.

4.1 Material properties and experimental set-up

The main component of the fill materials is CDG soil. Figure 6 presents the grain size distribution curves for the CDG samples taken from different boreholes and different elevations in the Guangming waste dump. The average values for the material properties of the CDG samples are listed in Table 2. The CDG soil was classified as a clayey sand [30].

All the CDG samples taken from the site were mixed to prepare the re-compacted specimens for the laboratory tests, and the experimental set-up is described in Table 3. As pointed out by OKA [12], the fully undrained test can simulate the behaviour of unsaturated soil during rapid loading. Unconsolidated and undrained (UU) triaxial tests were therefore carried out to simulate landfilling with a fast dumping rate and poor drainage. The escape of pore air and pore water was not permitted in these tests. However, the unsaturated specimens were partially consolidated due to

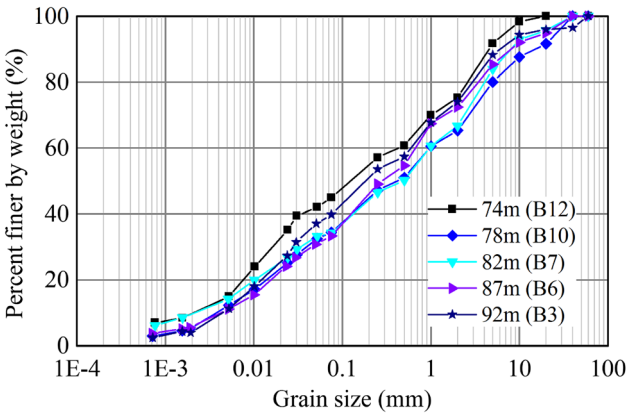

Fig. 6 Grain size distribution curves for the CDG soil samples taken from different locations in the Guangming waste dump

Table 2 Material properties of the CDG soil

G_s	ω_L (%)	ω_P (%)	ω_{op} (%)	ρ_{dmax} (g·cm^{-3})
2.68	39.7	20.5	12	1.89

Table 3 Scheme of the UU tests

Test type	Test group no.	Initial dry density (g/cm^3)	Water content	Initial saturation degree	Confining pressure (kPa)
UU	S1	1.3	19%	48%	50, 100, 200, 400, 800
	S2		23%	58%	
	S3		26%	66%	

the compressibility of the pore air. However, to avoid confusion, the term 'UU' is retained in this paper.

Conventional triaxial apparatus designed for a saturated soil was used for the UU tests. The confining pressure increased at a rate of 25 kPa/min in the isotropic compression stage until the target value was reached. Shearing was exerted at a high rate of 0.625 mm/min. Data were recorded at each 0.3% increment in vertical strain until the total strain reaches 25%. The pore pressure was measured by the pore-water pressure transducer connected to the bottom of specimen. It is pity that the pressures in pore air and pore water cannot be measured separately. So it is believed that the recorded pore pressure is the greater one between pore-air pressure and pore-water pressure. The pore-water pressure is close to the pore-air pressure for the specimens with high saturation degree, and therefore regarded as pressure of the pore fluid mixture.

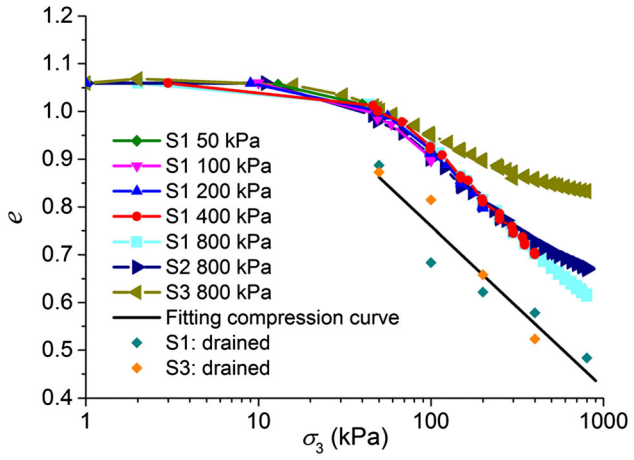

Fig. 7 e-log σ_3 curves from the UU tests on the unsaturated specimens and the isotropic compression curve of the specimens

4.2 Experimental results and analyses

Figure 7 presents the volume changes in the undrained isotropic compression stage. For the five S1 specimens with a saturation degree of 48%, the e-log σ_3 curves from the tests with different target values of confining pressure are consistent. The void ratios show a slight decrease with the increase in confining pressure less than 50 kPa and then decrease significantly with the further increase in confining pressure. The total volume changes for the S1, S2 and S3 specimens under a confining pressure of 800 kPa are 21.7%, 20% and 11.1%, respectively. A specimen with a lower saturation degree has a higher compressibility under undrained compression. Drained isotropic compression tests were also carried out for the S1 and S3 specimens. The compression curve was determined by fitting these experimental results and presented in Fig. 7 as a black line. It can be seen that all the e-log σ_3 curves from the undrained compression are above the drained compression curve. Therefore, the specimens were not completely consolidated under the undrained condition, and excess pore pressure generated and prevented further contraction of the samples. Based on the measured pore pressures, the values of pore pressure coefficient B were determined to vary from 0.11 to 0.42 for S1, 0.15 to 0.63 for S2 and 0.25 to 0.90 for S3. The values of pore pressure coefficient B are not constants due to the change in saturation degrees during the compression processes. The samples with a higher saturation degree initially have greater values of B.

The stress paths in terms of q versus p and q versus $(p-u)$ recorded in the shear stage are presented in Fig. 8. As shown in Fig. 8, further increase in pore pressure was observed at the shearing state since the difference between the total stress p and the effective stress $(p-u)$ increased with the increasing q. For S2 and S3, a slight increase in $(p-u)$ just before failure (see Fig. 8b and c) indicates a slight decrease in the pore pressure. The pore pressure coefficient $\overline{A}$, determined by $\overline{A} = \Delta u/Bq$, varies from 0.3 to 1.54 for S1, 0.37 to 1.88 for S2 and 0.36 to 1.34 for S3 with an increase in q. Δu is the change in the pore pressure in the undrained shear stage. It is found that the specimens with a higher initial saturation degree show a much lower deviatoric stress and a greater pore pressure at failure under the same confining pressure.

With an interpretation of the experimental results in accordance with the methodology of USA, the undrained shear strength c_u from each test was obtained and plotted against the normal stress σ_n on the failure plane in Fig. 9. The undrained shear strength increases nonlinearly, and the

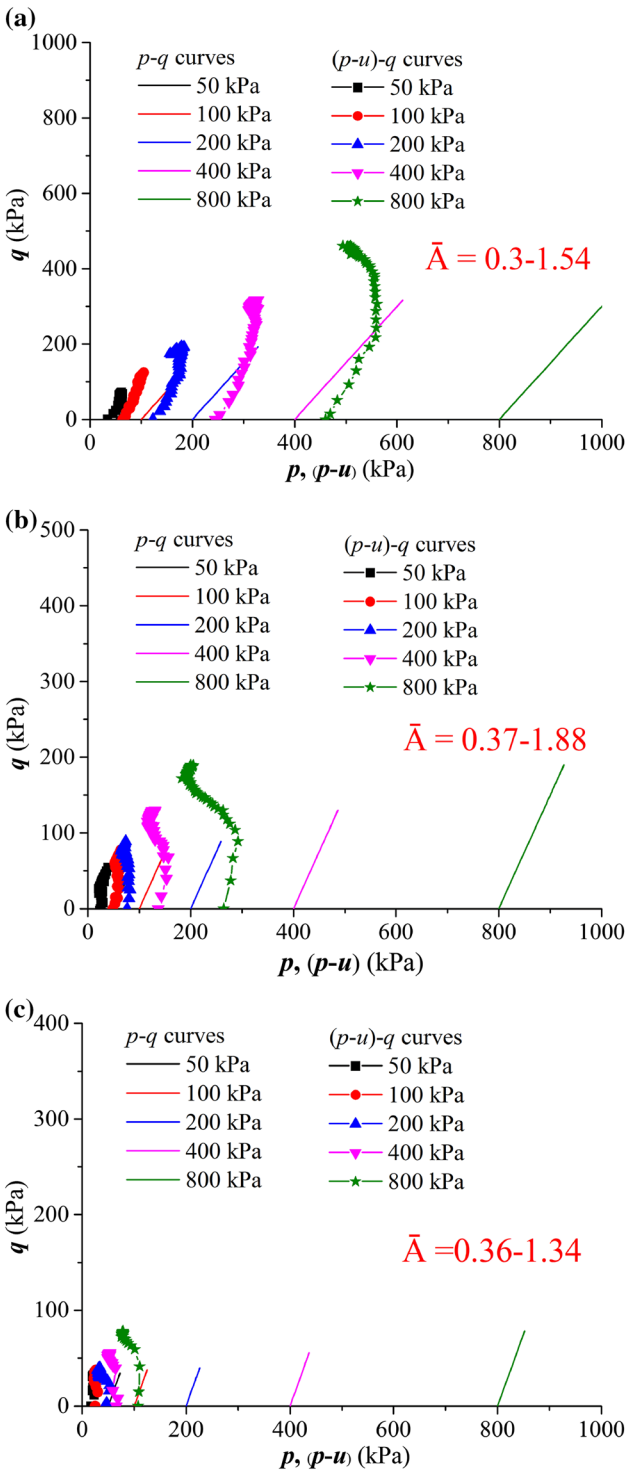

Fig. 8 Stress paths in the shearing stage of the UU tests for the test groups of (**a**) S1, (**b**) S2 and (c) S3

increasing rate decreases with increase in σ_3 (or σ_n). It is found that the specimens with a higher saturation degree present a much smaller increment of shear strength. Taking S3 as an example, c_u increases by only 20 kPa as the confining pressure increases from 50 to 800 kPa. The

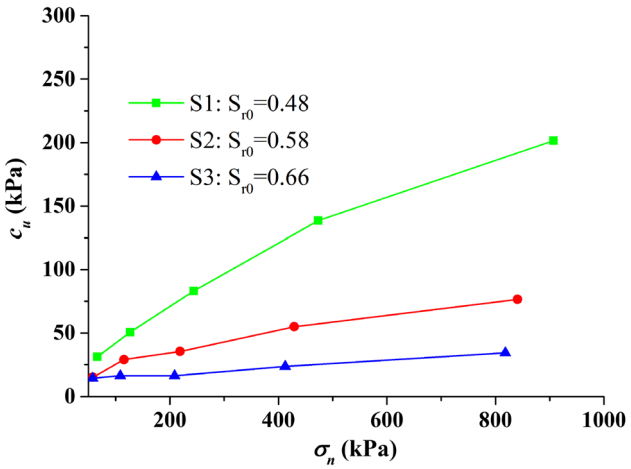

Fig. 9 Undrained shear strengths for the specimens with different initial saturation degrees

Table 4 Values of the effective strength parameters determined by the UU tests

Test group no	Water content (%)	Effective strength parameters	
		φ_1'(°)	c_1'(kPa)
S1	19	28.7	21.6
S2	23	24.8	19.1
S3	26	27.7	10.0

values of the effective strength parameters were determined based on the measured pore pressures and are listed in Table 4.

4.3 Comparison between measured and estimated shear strengths

The proposed estimation method of undrained shear strength was validated by comparing the estimated results with the measurements from the UU triaxial tests. The parameters for the estimation are listed in Tables 5 and 6. λ is determined as the slope of the segment of the isotropic compression curve with a confining pressure greater than 50 kPa. The $e - \ln\sigma_3'$ curve is converted from the $e - \log\sigma_3'$ curve shown in Fig. 7. κ is assumed equal to

Table 5 Parameters for the estimation of undrained shear strength

n_0	0.51	c'	17 kPa
k	0.02	w_r	15%
λ	0.14	α	0.05
φ'	28°	β	1.48

Table 6 Void ratio and compressibility of the soil skeleton under different confining pressures

Confining pressure (kPa)	0	50	100	200	400	800
Void ratio	1.06	0.718	0.655	0.595	0.528	0.464
$C_s/10^{-4}$ kPa^{-1}	–	17.5	13.9	6.14	2.70	1.50

$(1/10 \sim 1/5)$ of the value of λ [21]. The average values of the strength parameters listed in Table 4 were employed for φ' and c'. The residual water content w_r and the fitting parameters α and β were determined by the SWCC of the CDG. The void ratio under different confining pressures was also determined by the compression curve presented in Fig. 7. The values of C_s under different total confining pressures are determined by iterative calculations. For a given total confining pressure, σ_3, the pore pressure is assumed to be 0 in the beginning of the iterative calculation, and therefore, the effective confining pressure σ_3' is equal to σ_3. The initial value of C_s is determined by the initial value of σ_3' and the e- σ_3' curve converted from the e-log σ_3' curve. The value of C_s is employed in Eq. (4) to calculate the increment of pore pressure. The σ_3' will be calculated based on the updated pore pressure and will lead to a new value of C_s. The operations will be repeated till the obtained pore pressure has a difference less than 0.1 with the value determined in the former step. The value of C_s determined in the last step is listed in Table 6, together with the total stress σ_3 given in the beginning.

Figure 10 presents the estimated and measured pore pressures in the undrained isotropic compressions. The estimated values for the S3 specimens with an initial saturation degree of 66% fit well with the measurements, while the pore pressures for S1 and S2 are overestimated under a high confining pressure. In the case that the surface tension is disregarded, the compressibility of a water/air mixture is underestimated based on the general expression derived by Schuurman [14]. In other words, the pore pressure coefficient B is overestimated by Eq. (1). The overestimation is greater for a specimen with a lower saturation degree.

A comparison between the measured and estimated undrained shear strengths is shown in Fig. 11. The solid lines represent the estimated shear strengths without considering the contribution from suction, while the dashed lines take the suction into account. The suction-induced stress σ_s was assumed equal to $S_e(u_a - u_w)$, being a part of the effective consolidation stress. The estimated strength for the S3 specimen with an initial saturation degree of 66% fits well with the measurement when the contribution of suction is not taken into account. The result considering the contribution of suction is slightly greater than the experimental data, especially under a low confining pressure. Therefore, the contribution of suction for S3 is overestimated. The shear strengths of S1 and S2 are underestimated due to the overestimation of the pore pressure in the compression stage and the assumption that no volume change occurs in the shear stage. The estimation considering the contribution of suction for S1 and S2 agrees more closely with the measurements under low confining pressures. The effect of suction diminishes gradually with increase in confining pressure. This comparison between the estimated and measured shear strengths indicates that the proposed estimation method is applicable for the CDG fill with a saturation degree greater than 0.6.

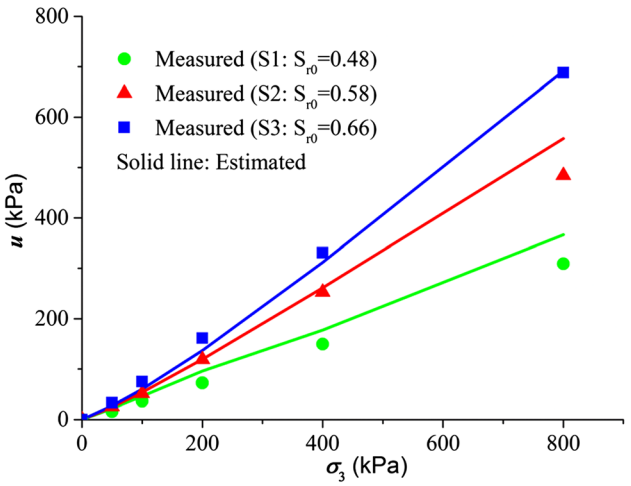

Fig. 10 Comparison between the measured and predicted pore pressures under undrained isotropic compression

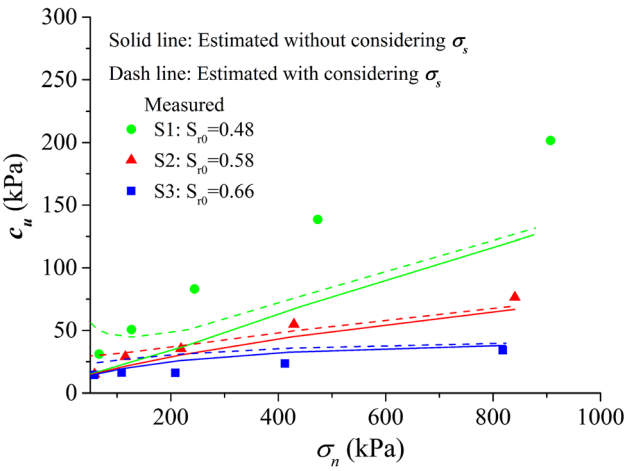

Fig. 11 Comparison between the measured and estimated undrained shear strengths

5 Total stress based stability analysis

Based on the interpretation of stress paths during landfilling and the shear strength estimation method, the values of undrained shear strength for the fill materials in different zones can be determined and correlated with the total normal stress on the potential failure surface. The total stress-based stability analysis is thus implementable for the landslide in the Guangming waste dump.

5.1 Limit equilibrium analysis of the waste dump

5.1.1 Stability analysis using the measured shear strength curves

The measured shear strength curves from the UU tests were employed in the limit equilibrium analysis of the waste dump via the software GEO-SLOPE. The c_u versus σ_n curves of S1, S2 and S3 presented in Fig. 9 were applied to define the strength property of fill materials in the low water content zone, the transition zone and the high water content zone, respectively. GEO-SLOPE provides a shear/normal strength function to implement a nonlinear relationship between c_u and σ_n. The total normal stress on the potential failure surface, σ_n, is determined by the software based on the topography of the slope and the density of the fill. Thus, the shear strength c_u can be specified by the c_u versus σ_n curves and the value of σ_n. Morgenstern-Price method was used to calculate the FOS for the potential failure surfaces. As shown in Fig. 12, the FOS was calculated to be 0.741 for the most critical slip surface, which was optimized by the software based on the specified slip surface according to the one identified in the field investigation (see Fig. 1). The optimized critical slip surface is deep-seated and passes through the lower zone with a high water content.

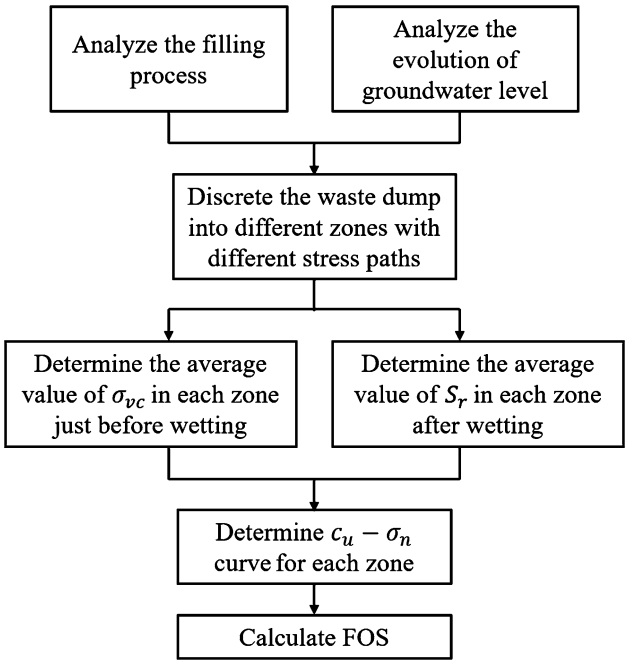

Fig. 13 Flow chart of the stability analysis based on the estimation method of undrained shear strength

5.1.2 Stability analysis using the estimated shear strengths

The procedure of stability analysis using the estimated undrained shear strength is indicated in Fig. 13. The filling process of the waste dump was analysed to determine the loading history and the initial saturation degree for different parts. The evolution of groundwater level was determined by seepage analysis. The waste dump was then discreted based on the initial saturation degree and the groundwater levels computed at different stages. Each of the discrete zones had a unique stress path and hence a unique shear strength evolution during landfilling. The timing of wetting was reflected by the value of vertical total stress σ_{vc} for a given zone just before wetting. The average value of σ_{vc} for a given zone was determined as the

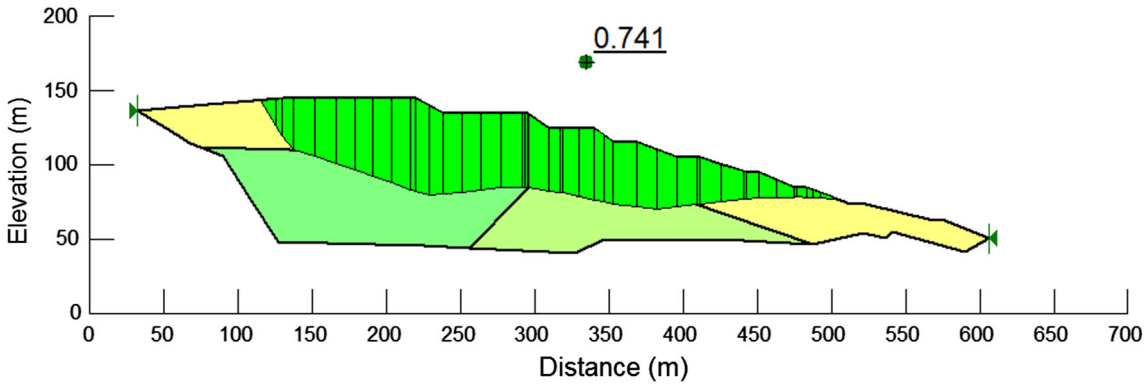

Fig. 12 Result of the stability analysis of the Guangming waste dump using the measured shear strength curves

self-weight of the soil column above the slip surface. The equivalent confining pressure was then calculated by $\sigma_3 = \sigma_{vc}(1 + 2K_0)/3$. K_0 was estimated by $1 - \sin\varphi'$. The average value of internal friction angle φ' in Table 5 was used. The saturation degree of each zone after wetting was determined from the suction computed from the seepage analysis by referring to the SWCC of CDG. The c_u versus σ_n curves for different zones were determined by the estimation method and employed to calculate the FOS.

As discussed previously, the Guangming waste dump was discreted into fourteen zones as shown in Fig. 3. The values of σ_{vc} and σ_3 for the fourteen zones were estimated by analysing the filling process and listed in Table 7. Figure 14 presents the shear strengths estimated for three representative zones. The dashed lines represent the shear strengths of the fill without considering the wetting process. The solid lines are the shear strengths of the fill subjected to wetting. The dot-dashed lines are the estimated strengths without considering the contribution of suction. It is noticeable that the solid lines are consistent with the dashed lines before wetting and show a sudden drop after wetting. For the fill in zone 2 located in the lower and wet layer of the waste dump, the increase in shear strength with surcharge loading is limited before wetting. The subsequent wetting makes the fill saturated. The shear strength of the saturated fill then remains constant with further surcharge loading. For the fill in zone 12, which has a lower initial saturation degree than those of other zones, the fill keeps unsaturated after the wetting process. The solid line then deviates from the dashed line, and their difference becomes significant with further surcharge loading. The shear strength of the lower and wet zones is significantly limited by a build-up of excess pore pressure due to the high initial saturation degree and rapid filling. The wetting of the fill material with a low initial saturation degree results in a significant decrease in the rate of increase in the shear strength with further surcharge loading.

The fourteen curves of c_u versus σ_n obtained from the estimation method were applied to determine the strengths of fill in the fourteen zones. For a given zone, the total normal stress σ_n on the slip surface was computed and used to determine c_u by the software GEO-SLOPE automatically. The unit weight after wetting was used to compute

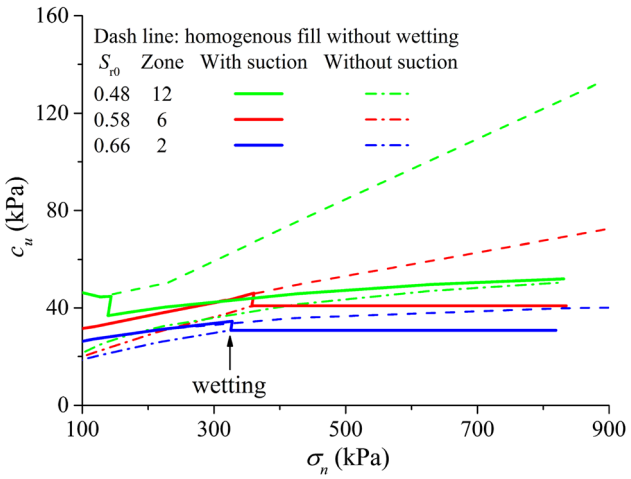

Fig. 14 Undrained shear strengths of the three representative zones

σ_n. The results of the stability analyses performed using the estimated strengths with and without considering the contribution of suction are indicated in Fig. 15a and b. The corresponding FOSs calculated for the slip surface identified by the field investigation are 0.896 and 0.775, respectively. Suction has a notable impact on the stability of the initially unsaturated waste dump fill. Although the estimated shear strength for the low-water-content zone is less than the measured value, the FOS using the estimated strength and considering the contribution of suction is slightly greater than the result using the measured strength. This result implies that the slope stability is more sensitive to the shear strength in a zone with a higher water content. It is believed that the FOS with considering the suction will be more close to 1 when the three-dimensional effect of the real slope is taken into account.

The stability analyses based on the undrained shear strengths clarified the failure mechanism of the Guangming landslide: The gain of shear strength with the surcharge loading in the lower and wet layer of the waste dump was limited by a build-up of excess pore-water pressure. The gain of shear strength for the upper and relatively dry fill material was attenuated with the rise of groundwater level. When the shear strength was not enough to resist the increasing slip force with the surcharge loading, a deep-seated translational failure took place in the lower and wet layer of the waste dump. The stability analyses also

Table 7 The average value of vertical stress and equivalent confining pressure for the fourteen zones just before wetting

Zone	1	2	3	4	5	6	7	8	9	10	11	12	13	14
σ_{vc}(kPa)	867	446	199	212	783	484	310	232	527	301	265	170	345	232
σ_3(kPa)	596	306	136	146	538	333	213	159	362	207	182	116	237	159

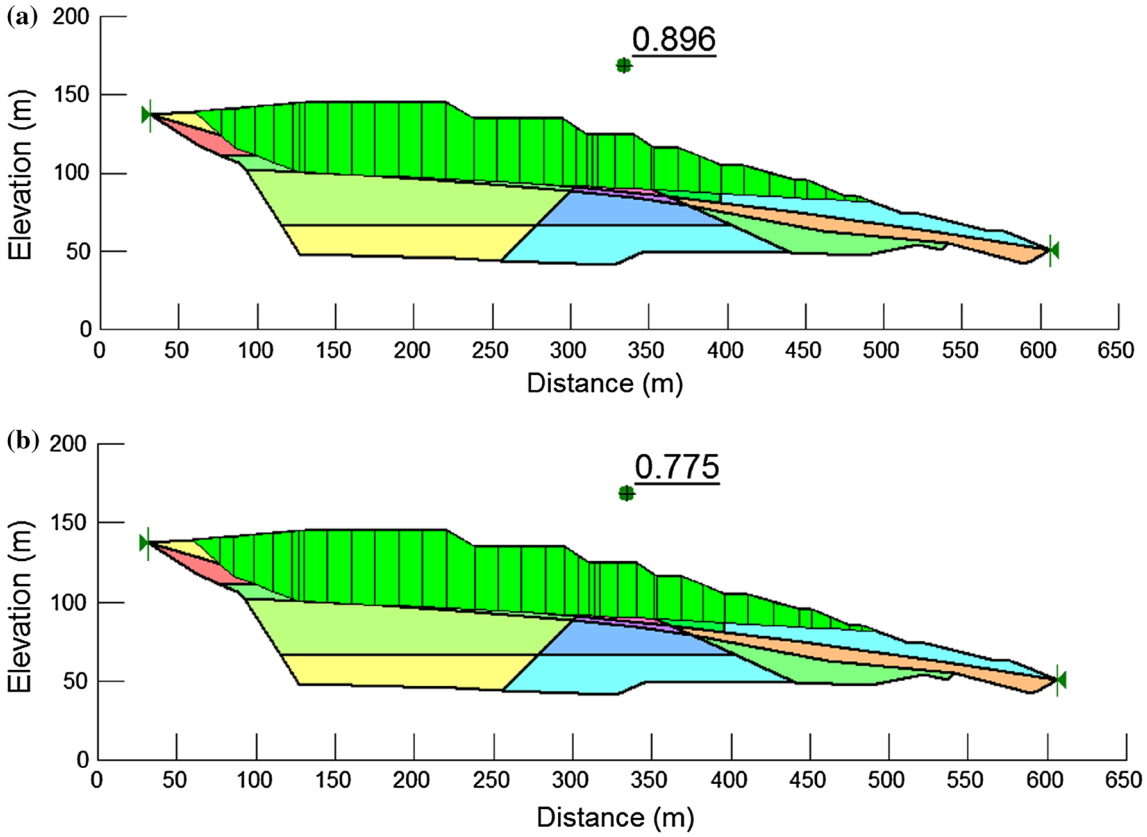

Fig. 15 Results of stability analyses using predicted undrained shear strengths (**a**) with or (**b**) without considering the contribution of suction

demonstrated that the proposed estimation method for undrained shear strength is required for the landfilling with a complex stress path involving both surcharge loading and wetting. However, for the case with only surcharge loading, it is more rational to perform UU triaxial tests to determine the undrained shear strength.

5.2 Effect of water content on the landfill height and capacity

As indicated before, the gain of undrained shear strength is dependent on the initial water content of fill materials. The effect of the water content on the height and capacity of a landfill was studied via total stress-based stability analyses. Two scenarios of landfilling were analysed. In the first scenario, the fill material has a uniform water content. In the second scenario, the high-water-content fill and low-water-content fill are dumped in the back and front zones, respectively (see Fig. 18). The simplified calculation model for the landfill capacity is shown in Fig. 16. For the longitudinal length $L \geq Hn$, the expression for calculating capacity is $V = (2L - Hn)HW/2$. The critical height of landfill H was determined when the FOS was equal to 1.15 in the stability analysis. The undrained shear strengths obtained from the UU tests were used in the stability analyses.

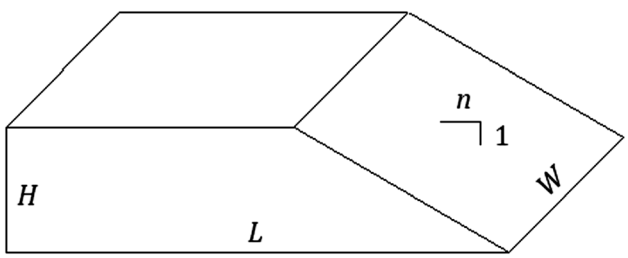

Fig. 16 Calculation model of landfill capacity

5.2.1 Scenario 1: rapid filling of uniform CDG soil

In this scenario, the fill is CDG with a uniform water content. As shown in Fig. 17a, the limit of fill height decreases with increase in slope inclination. For a given slope inclination, the fill with an initial water content of 19% presents a much greater height limit than the fills with higher water contents. Figure 17b shows the landfill capacity results estimated for a waste dump with a length of 400 m. The low-water-content fill has a higher height limit and thus a greater landfill capacity. For a water content of 19%, the calculated landfill capacity is maximized at a slope inclination of 1:3. The landfill capacity for

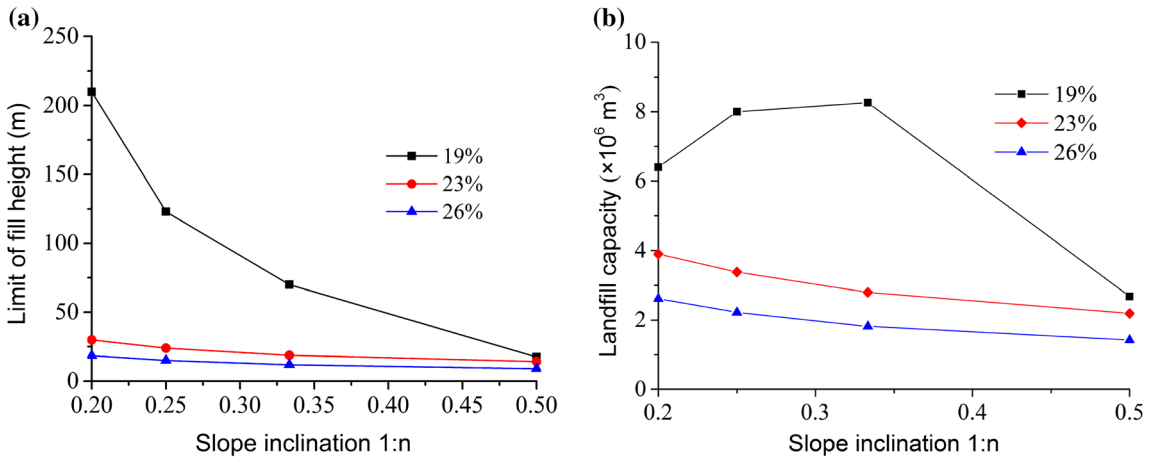

Fig. 17 Landfill heights and capacities for uniform CDG with different initial water contents: (**a**) limit of fill height and (**b**) landfill capacity

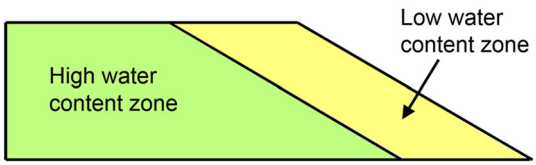

Fig. 18 Model for stability analysis of slopes with two zones with different water contents

the fill with a higher water content monotonically decreases with an increase in slope inclination.

5.2.2 Scenario 2: rapid filling of CDG with two different values of water content

In the case of two zones with different water contents, the low-water-content fill is dumped in the front area as a retaining dam. The high-water-content fill is then dumped at the back. This operation is repeated in layered landfilling to form a two-zone structure, as shown in Fig. 18. It was assumed that the initial water contents for the two zones are 19% and 26%, respectively.

Figure 19 shows the dependency of landfill height and capacity on the width of the low-water-content zone. As shown in Fig. 19a, for the inclination of 1:3, the limit of fill height increases as the low-water-content zone widens. The limit of fill height ultimately reaches a constant value that is equal to the limit of height for landfilling with only low-water-content fill. In Fig. 19b, the landfill capacity shows a positive correlation with the width of the low-water-content zone. For a given inclination, the waste dump with a greater length has a higher capacity due to its larger size.

6 Conclusions and suggestions

This paper presents a quantitative analysis of the failure mechanism of the catastrophic landslide in Shenzhen. Seepage analyses in the waste dump were conducted to compute the rise of groundwater level during the filling

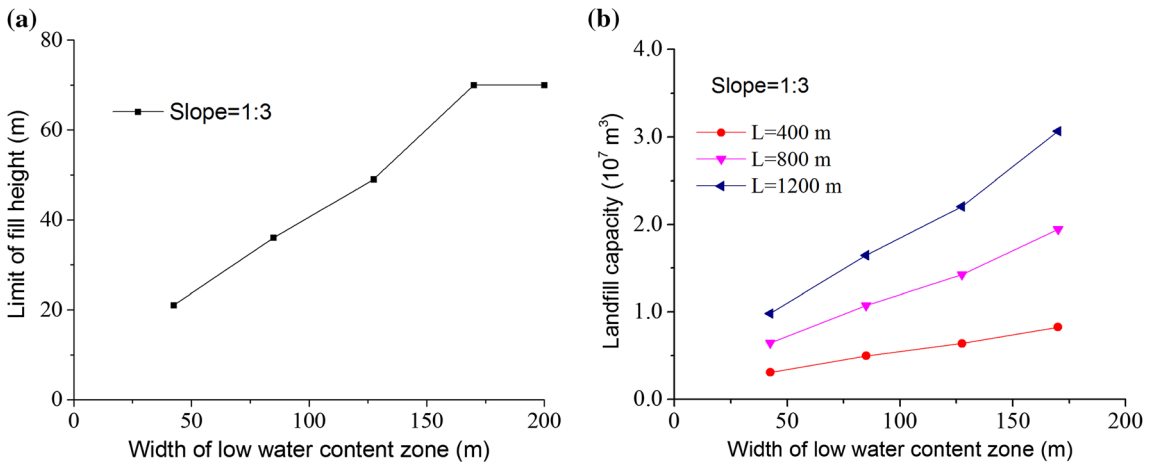

Fig. 19 Landfill heights and capacities for fills with two zones with different water contents: (**a**) limit of fill height and (**b**) landfill capacity

process, and the complex stress paths involving both rapid filling and wetting were investigated. The undrained shear strength of unsaturated fill under the complex stress paths was estimated by using the simplified method proposed, and the estimation was validated by the UU triaxial tests. Total stress-based stability analysis was carried out to calculate the factor of safety of this waste dump at failure. The following conclusions and suggestions are drawn from this study.

a. The gain of the undrained shear strength for the fill materials in the waste dump depends on both the surcharge loading resulting from the dumping operation and the wetting caused by the rise of the groundwater level. Based on the methodology of undrained strength analysis, a simplified method was proposed for the estimation of undrained shear strength for the case with a complex stress path involving both surcharge loading and wetting. The estimation method is proven to be more accurate for the CDG fill with a higher initial saturation degree.
b. The undrained shear strength increases nonlinearly with an increase in confining pressure for the unsaturated fill. The gain of shear strength of the fill material with a high initial saturation degree is much less than that of the fill with a low initial saturation degree. The subsequent wetting on the fill material with a low initial saturation degree results in a significant decrease in the rate of increase in shear strength with surcharge loading.
c. The total stress-based stability analysis based on the predicted c_u versus σ_n curves is proven to be applicable to waste-dumping operations with rapid filling and a rising groundwater level. The stability analyses indicated the failure mechanism: the gain of shear strength with the surcharge loading in the lower and wet layer of the waste dump was limited by a build-up of excess pore-water pressure. The gain of shear strength for the upper and relatively dry fill material was attenuated with the rise of groundwater level. When the shear strength was not enough to resist the increasing slip force with the surcharge loading, a deep-seated translational failure took place in the lower and wet layer of the waste dump.
d. In the rapid filling of uniform fill material, the limit of fill height has a negative correlation with the initial water content. The landfill capacity tends to maximize at a slope inclination of 1:3. For the input materials with two water contents, a two-zone waste dump structure is suggested, and the landfill capacity shows a positive correlation with the width of the front zone with a low water content.

Acknowledgements The authors express their gratitude to Professors Yu-jun Cui, Cheng-gang Bao and De-an Sun for their technical advices to this manuscript.

Funding The research for this paper was financially supported by the National Natural Science Foundation of China (Grant Nos. 51809230 and 51625805) and Key R&D Project of Zhejiang Province (Grant No. 2019C03107).

Compliance with ethical standards

Conflict of interest The authors declare that they have no conflict of interest.

References

1. Chen L-h, Chen Z-y (2003) Identification of soil parameters of extended Cambridge model and its application to Xiaolangdi project. Geomechanics 24(2):229–232
2. Chen Z-Y (2003) Principles, methods and procedures of soil slope stability analysis. China Water Resources and Hydropower Press
3. Gao Y, Yin Y, Li B, Wang W, Zhang N, Yang C, Zuo X (2017) Investigation and dynamic analysis of the long runout catastrophic landslide at the Shenzhen landfill on December 20, 2015, in Guangdong, China. Environ Earth Sci 76(1):13. https://doi.org/10.1007/s12665-016-6332-8
4. Van Genuchten M (1980) A closed-form equation for predicting the hydraulic conductivity of unsaturated soils1. Soil Sci Soc Am J. https://doi.org/10.2136/sssaj1980.03615995004400050002x
5. Jin Y, Yuan W, Yin Z, Cheng YM (2019) An edge-based strain smoothing particle finite element method for large deformation problems in geotechnical engineering. Int J Numer Anal Methods Geomech 44:923–941
6. Ladd C (1991) Stability evaluation during staged construction. J Geotech Eng. https://doi.org/10.1061/(ASCE)0733-9410(1991)117:4(540)
7. Li D, Sun Z-q, Su Y, Zhou D, Qi H (2018) Current situation and strategy analysis of residual sludge in Shenzhen. Constr Technol 47(S3):134–136
8. Liang H, He S, Lei X, Bi Y, Liu W, Ouyang C (2017) Dynamic process simulation of construction solid waste (CSW) landfill landslide based on SPH considering dilatancy effects. Bull Eng Geol Env 78(2):763–777. https://doi.org/10.1007/s10064-017-1129-x
9. Lowe J (1967) Stability analysis of embankments. J Soil Mech Found Div 93(4):1–33
10. Lu N, Asce M, Likos W (2006) Suction stress characteristic curve for unsaturated soil. J Geotech Geoenviron Eng. https://doi.org/10.1061/(ASCE)1090-0241(2006)132:2(131)
11. Lu N, Godt J, Wu D (2010) A closed form equation for effective stress in unsaturated soil. Water Resour Res. https://doi.org/10.1029/2009WR008646
12. Oka F, Kodaka T, Suzuki H, Kim Y, Nishimatsu N, Kimoto S (2010) Experimental study on the behavior of unsaturated compacted silt under triaxial compression. Soils Found 50:27–44. https://doi.org/10.3208/sandf.50.27
13. Ouyang C, Zhou K, Yin J, Peng D, Wang D, Li W-l (2017) Dynamic analysis and numerical modeling of the 2015 catastrophic landslide of the construction waste landfill at Guangming, Shenzhen, China. Landslides. https://doi.org/10.1007/s10346-016-0764-9

14. Schuurman IE (1967) The compressibility of an air/water mixture and a theoretical relation between the air and water pressures. Geotech Lond Engl 16(4):269–281
15. Shi Z-j, Wang Y-h, Xu L-h, Xiong W, Yu P-t, Hu Z-s, Gao J-x (2009) Effect of topographic form and vegetation type on the runoff coefficient in the Xiangshuihe watershed of Liupan Mountains. Sci Soil Water Conserv 7(4):31–37
16. Shi B, Zhang Y, Zhang W (2017) Run-out of the 2015 Shenzhen landslide using the material point method with the softening model. Bull Eng Geol Env 78(2):1225–1236. https://doi.org/10.1007/s10064-017-1167-4
17. Skempton A (1954) The pore-pressure coefficients A and B. Geotechnique 4:143–147. https://doi.org/10.1680/geot.1954.4.4.143
18. Skempton AW, Bishop AW (1954) Building materials, their elasticity and plasticity soils
19. Sun M (2007) Study on the relationships between the soil moisture condition of underlying surface and rainfall-runoff. J Shanxi Univ Nat Sci Ed 30(1):131–134
20. Vanapalli S, Fredlund DG, Pufahl DE, Clifton AW (1996) Model for the prediction of shear strength with respect to soil suction. Can Geotech J 33:379–392. https://doi.org/10.1139/t96-060
21. Wang C-M (2015) Soil mechanics. Geological Press
22. Xie L-c, Chen J-y, Fu C-s, Huang X-l, Jiang H-b, Dong L-y, Chen Z-l (2011) Observation and analyses of groundwater recharge from rainfall infiltration in a coastal watershed, south China. Ecol Ecol Environ Sci 20(Z2):1259–1267
23. Xu Q, Peng D, Li W-l, Dong X, Hu W, Tang M, Liu F (2017) The catastrophic landfill flowslide at Hongao dumpsite on December 20 2015 in Shenzhen, China. Nat Hazards Earth Syst Sci Discuss 17:277–290. https://doi.org/10.5194/nhess-17-277-2017
24. Yang J, Yin Z, Laouafa F, Hicher PY (2018) Internal erosion in dike-on-foundation modeled by a coupled hydromechanical approach. Int J Numer Anal Meth Geomech 43(4):1–21
25. Yang J, Yin Z, Laouafa F, Hicher PY (2019) Modeling coupled erosion and filtration of fine particles in granular media. Acta Geotech 14:1615–1627. https://doi.org/10.1007/s11440-019-00808-8
26. Yang J, Yin Z, Laouafa F, Hicher PY (2019) Analysis of suffusion in cohesionless soils with randomly distributed porosity and fines content. Comput Geotech 111:157–171
27. Yang J, Yin Z, Laouafa F, Hicher PY (2020) Three-dimensional hydromechanical modeling of internal erosion in dike-on-foundation. Int J Numer Anal Methods Geomech 44(8):1200–1218
28. Yang J, Yin Z, Laouafa F, Hicher PY (2020) Hydromechanical modeling of granular soils considering internal erosion. Can Geotech J 57:157–172
29. Yin Y, Li B, Wang W, Zhan L, Xue Q, Gao Y, Zhang N, Chen H, Liu T, Li A (2016) Mechanism of the December 2015 catastrophic landslide at the shenzhen landfill and controlling geotechnical risks of urbanization. Engineering 2(2):230–249. https://doi.org/10.1016/J.ENG.2016.02.005
30. Zhan L-t, Zhang Z, Chen Y-m, Chen R, Zhang S, Liu J, Li A-g (2018) The 2015 Shenzhen catastrophic landslide in a construction waste dump: reconstitution of dump structure and failure mechanisms via geotechnical investigations. Eng Geol 238:15–26. https://doi.org/10.1016/j.enggeo.2018.02.019
31. Zhu, C, Huang Y, Zhan L (2018) SPH-based simulation of flow process of a landslide at Hongao landfill in China. Nat Hazards 1–14